
PUSH-FORWARD SIGNED DISTANCE FUNCTIONS ENABLE INTERPRETABLE AND ROBUST CONTINUOUS SHAPE QUANTIFICATION

A PREPRINT

Roua Rouatbi^{1,2,3,4}
rouatbi@mpi-cbg.de

Juan Esteban Suarez^{2,3}
suarez@mpi-cbg.de

Ivo F. Sbalzarini^{1,2,3,4,5}
sbalzarini@mpi-cbg.de

¹Dresden University of Technology, Faculty of Computer Science

²Max-Planck Institute of Molecular Cell Biology and Genetics

³Center for Systems Biology Dresden

⁴Center for Scalable Data Analytics and Artificial Intelligence Dresden/Leipzig

⁵Cluster of Excellence “Physics of Life”, TU Dresden

ABSTRACT

We introduce the Push-Forward Signed Distance Morphometric (PF-SDM), a novel method for shape quantification in biomedical imaging that is continuous, interpretable, and invariant to shape-preserving transformations. PF-SDM effectively captures the geometric properties of shapes, including their topological skeletons and radial symmetries. This results in a robust and interpretable shape descriptor that generalizes to capture temporal shape dynamics. Importantly, PF-SDM avoids certain issues of previous geometric morphometrics, like Elliptical Fourier Analysis and Generalized Procrustes Analysis, such as coefficient correlations and landmark choices. We present the PF-SDM theory, provide a practically computable algorithm, and benchmark it on synthetic data.

Keywords Geometric shape analysis · level-set methods · Shape quantification · Morphometric

1 Introduction

The human visual system excels at recognizing and grouping similar-looking objects based on their shape, forming equivalence classes invariant to shape-preserving transformations such as rotation, translation, reflection, and scaling. For instance, the outline of a flower may be perceived as more similar to a star than to a circle. Capturing this cognitive ability in a quantitative measure of shape similarity is a significant open challenge in biomedical imaging. Such measures, called morphometrics, have long been studied to quantify shape differences, with methods such as Generalized Procrustes Analysis (GPA) [12], Elliptical Fourier Analysis (EFA) [6], achieving significant success [19], or more recent methods, such as Euler Characteristic Transform (ECT) and Persistent Homology Transform (PHT) [21]. However, EFA suffers from coefficient interdependence and sensitivity of the description to the starting tracing point. These limitations hamper EFA’s interpretability and robustness. Also, GPA faces robustness issues due to its reliance on (usually manually) selected landmark points. Discrete or topological methods, like ECT or PHT, do not provide access to smooth geometric features like curvature. Due to these limitations of classic morphometrics, approaches based on Signed Distance Functions (SDF) [14] have been proposed to enable a more nuanced understanding of geometry from which interpretable geometric quantities can be derived [9]. The SDF measures the orthogonal distance from

This work has been submitted to the IEEE for possible publication. Copyright may be transferred without notice, after which this version may no longer be accessible.

any point in a domain to the boundary of the shape by solving the Eikonal equation [15] or the level-set equation [17]. The singularities in the solution of the Eikonal equation characterize the topological skeleton of a shape, shown to be a successful measure for shape similarity [11]. However, due to the nonlinearity of the Eikonal equation, the complexity of boundary conditions, and singularities in the solution, most SDF methods are limited to discrete representations of the SDF that are not invariant to shape-preserving transformations.

Here, we present a continuous and interpretable morphometric that efficiently captures geometric features of shapes while remaining invariant to rotation, translation, reflection, and scaling. Specifically, we introduce the Push-Forward SDF (PF-SDF) as a modified SDF defined over a global reference domain for all shapes. Leveraging this, we develop a geometric morphometric, termed the PF-SDM, based on the angular moments of the PF-SDF’s curvature. The PF-SDM is designed to highlight topological differences between shape skeletons, radial symmetries, and curvature variations.

2 Method

The PF-SDM algorithm consists of four stages: image pre-processing 2.1, SDF computation 2.2, PF-SDF computation 2.3, and morphometric evaluation 2.4. We discuss these four steps in detail below, considering a set of N images, $I_n \subseteq \mathbb{R}^{p \times p}$, each containing p^2 pixels and representing N distinct shapes $\mathbb{S} \subseteq \Omega$. The set of shapes, $\mathbb{S} = \{S_i\}_{i=1}^N$, consists of closed, smooth, one-dimensional manifolds [5] embedded in the two-dimensional domain $\Omega := (-1, 1)^2$.

2.1 Image pre-processing

The image pre-processing stage consists of segmenting each input image such that the shape contour is isolated from the rest of the image (see Fig. 1). For simple shapes, we use the OpenCV [8] thresholding and contour finding methods. For more complex shapes and real-world microscopy images, we use the Segment Anything Model [16]. Finally, the points on the shape outline are scaled to $(-1, 1)$, matching Ω .

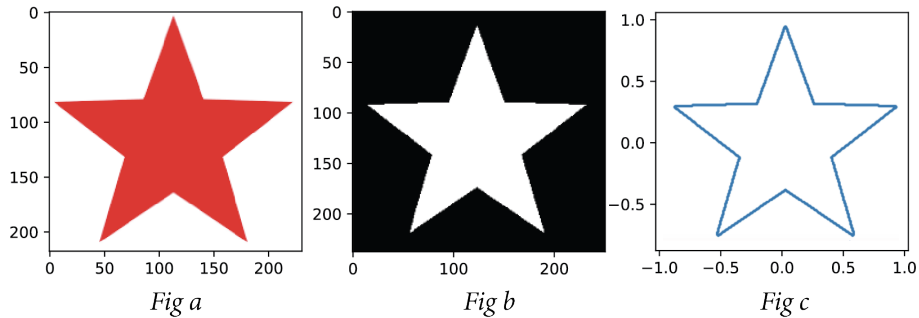


Figure 1: Image pre-processing pipeline: an input image (a) is segmented into fore- and background (b) and the contour is extracted (c).

2.2 Signed Distance Function computation

In the second stage, we compute the signed distance function $\phi : \Omega \rightarrow \mathbb{R}$ for a given shape S by solving the viscous Eikonal equation [2]. The viscosity term $\nu = 0.2$ helps smooth the solution around singularities. We thus solve:

$$\begin{cases} \|\nabla \phi(x, y)\|_2^2 + \nu \Delta \phi(x, y) = 1 & (x, y) \in \Omega, \\ \phi(x, y) = 0 & (x, y) \in S, \end{cases} \quad (1)$$

where $\|\cdot\|_2$ denotes the ℓ^2 -norm of a vector. The boundary condition for Eq. (1) is given by the M scaled contour points $\{x_i, y_i\}_{i=1}^M$ from the previous step. Note that, due to the ℓ^2 term, the Eikonal equation results in a nonlinear PDE. To overcome this challenge, we solve it numerically using Polynomial Surrogate Models (PSMs) [1]. Specifically, we find the solution PSM $\hat{u}_{\xi^*} \in \Pi_n(\Omega)$ by minimizing

$$\mathcal{L}[\hat{u}_{\xi}] := \int_{\Omega} (\partial_x \hat{u}_{\xi}^2 + \partial_y \hat{u}_{\xi}^2 + \nu \Delta \hat{u}_{\xi} - 1)^2 dx dy + \int_S (\hat{u}_{\xi}|_S)^2 ds, \quad (2)$$

where $\hat{u}_\xi|_S$ denotes the restriction of the PSM \hat{u}_ξ to the manifold S , and $\Pi_n(\Omega) := \text{Span}(\{x^i y^j\}_{i,j=1}^n)$ is the space of polynomials of degree n , spanned by the canonical monomial basis $\{x^i y^j\}_{i,j=1}^n$. For a detailed description of the algorithm for stably and accurately inferring optimal PSMs, we refer to Refs. [1, 4].

2.3 Push-Forward Signed Distance Function

The SDF ϕ_S completely characterizes the geometry of the shape S (since it is unique), is continuous, and enables computing geometric features, such as curvature [9, 3]. However, it is not invariant to shape-preserving transformations, mainly due to the lack of a global and robust notion of orientation and position. We address the shape-preserving invariance by introducing the PF-SDF $\tilde{\phi}_S : B_0 \rightarrow \mathbb{R}$ defined over a reference domain $B_0 \subseteq \Omega$, which “deforms” the SDF ϕ_S such that its zero level set coincides with the boundary of B_0 , i.e., $\partial B_0 = \{(x, y) : \tilde{\phi}_S(x, y) = 0\}$. This is called a “push-forward map” of ϕ_S . By mapping the SDF onto a reference, the push-forward map provides a scale- and translation-invariant representation of the original shape S , normalizing its geometric features. Here, we consider B_0 to be the unit disk in polar coordinates, $B_0 := \{(\theta, r) \in (0, 2\pi) \times (0, 1)\}$, with boundary $\partial B_0 = \{(\theta, r) \in B_0 : r = 1\}$ corresponding to the unit circle. The push-forward map of the SDF onto B_0 is efficiently computed as the deformation map of the PSM $\nu_\zeta := (\nu_{\zeta_x}, \nu_{\zeta_y}) : S \rightarrow \mathbb{R}^2$ with $\nu_{\zeta_x}, \nu_{\zeta_y} \in \Pi_m(\Omega)$ minimizing the loss

$$\mathcal{L}[\nu_\zeta] := \int_{\Omega} (\nu_{\zeta_x}(x, y) - x_b^*)^2 + (\nu_{\zeta_y}(x, y) - y_b^*)^2 dx dy, \quad (3)$$

where $(x_b^*, y_b^*) \subseteq \partial B_0$ is the closest-point projection [10] of a point $(x, y) \in S$ onto the boundary ∂B_0 , given by:

$$(x_b^*, y_b^*) := \arg \min_{(x_b, y_b) \in \partial B_0} (x - x_b)^2 + (y - y_b)^2. \quad (4)$$

We then define the PF-SDF for the unit-circle reference as:

$$\tilde{\phi}_S(\theta, r) := \phi_S(\Psi_x(\theta, r), \Psi_y(\theta, r)), \quad (5)$$

with the push-forward maps

$$\Psi_x(\theta, r) := r \cos(\theta) + \nu_{\zeta_x}(r \cos(\theta), r \sin(\theta)), \quad (6)$$

$$\Psi_y(\theta, r) := r \sin(\theta) + \nu_{\zeta_y}(r \cos(\theta), r \sin(\theta)). \quad (7)$$

This normalizing mapping is illustrated visually in Fig. 2 for the SDF of the star shape from Fig. 1.

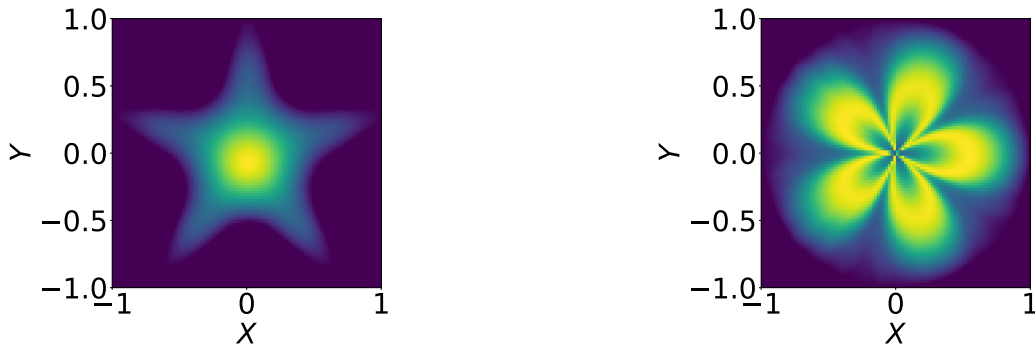


Figure 2: Illustration of the push-forward map of a SDF (left) to the corresponding PF-SDF with the unit circle as reference shape (right). This normalizes for scaling and translation.

2.4 Morphometric evaluation

The PF-SDF maps all shapes to a common domain where $r = 1$ is the shape boundary and $r = 0$ its center. This guarantees scale and translation invariance, while preserving the geometric information of an SDF approach. It thus

allows deriving similarity measures between the PF-SDFs $\tilde{\phi}_{S_i}, \tilde{\phi}_{S_j}$ of two shapes S_i, S_j that serve as morphometrics. Here, we propose a morphometric based on the angular moments of the curvature of the PF-SDF.

We start from the definition of the curvature $\kappa_S : [0, 2\pi] \times (0, 1) \rightarrow \mathbb{R}_+$ of the hypergraph $(\theta, \tilde{\phi}_S(\theta, \cdot))$:

$$\kappa_S(\theta, r) := \frac{|\partial_\theta^2 \tilde{\phi}_S(\theta, r)|}{(1 + \partial_\theta \tilde{\phi}_S(\theta, r)^2)^{3/2}}. \quad (8)$$

Note that this is not the curvature of the outline of the shape S , but rather the curvature of the PF-SDF everywhere in the embedding space Ω . The *curvature angular moments* $M_S^k : (0, 1) \rightarrow \mathbb{R}$ of order $k > 1$ for a shape S are then defined as:

$$M_S^k(r) := \frac{1}{2\pi} \int_0^{2\pi} (\kappa_S(\theta, r) - \bar{\kappa}_S(r))^k d\theta, \quad (9)$$

where $\bar{\kappa}_S : (0, 1) \rightarrow \mathbb{R}_+$ is the average curvature

$$\bar{\kappa}_S(r) := \frac{1}{2\pi} \int_0^{2\pi} \kappa_S(\theta, r) d\theta \quad (10)$$

for $r \in [0, 1]$. By convention, we set $M_S^1 := \bar{\kappa}_S$. From this, we define the K -th order PF-SDF morphometric $d_\phi^K : (S_1, S_2) \mapsto \mathbb{R}_+$ for two shapes $S_1, S_2 \subseteq \Omega$ as:

$$d_\phi^K(S_1, S_2) := \sum_{k=1}^K \frac{1}{m_k} \int_0^1 (M_{S_1}^k(r) - M_{S_2}^k(r))^2 dr, \quad (11)$$

where $m_k := \max_{r \in (0, 1), 1 \leq i \leq N} |M_{S_i}^k(r)|$ is the k -th moment normalizing constant. These morphometrics are rotational and reflection invariant as they solely rely on moments of the angular curvature. Moreover, since the PF-SDFs are defined to the reference shape B_0 , the functions $\kappa_{S_i}(r)$ can be compared pointwise for all $i = \{1, \dots, N\}$ without losing the invariances. As a result, the L^2 norm of these functions defines a distance between these quantities, as used in Eq. (11).

3 Results

We present two experiments that are designed to test the claimed properties of the PF-SDM. The first experiment examines how the PF-SDM supports interpretation of shape features. The second experiment assesses the morphometric's robustness under affine shape transformations. In both experiments, we use synthetic shapes for the sake of simplicity and clarity.

3.1 Experiment 1: Interpretability

We consider five different shapes: a star (S_1), an elongated ellipse-like shape (S_2), a circle (S_3), a square with rounded corners (S_4), and an asymmetric folded shape (S_5). To explore the behavior of the PF-SDM across these shapes, we compute the normalized moments $|\frac{1}{m_k} M_{S_i}^k(r)|$ for $k \in \{1, 2, 3\}$ across $r \in (0, 1)$. The results are shown in Fig. 3. In the right plot of Fig. 3, S_1 has high-frequency symmetric oscillations, corresponding to the radial symmetries of the star and the topology of its skeleton. In contrast, S_5 shows asymmetric oscillations, reflecting the asymmetric fold in this shape. S_2 presents a similar behavior as S_5 , but with a smaller magnitude and shifted asymmetries.

In the left and center plots, we observe that S_1 has larger moment magnitudes, which aligns with the star's higher curvature variations. Across all plots, S_3 and S_4 consistently display closer moments compared to the other shapes, reflecting the intuitive notion that the rounded square is most similar to the circle. Overall, the observed behaviors across the plots reinforce the expected relationships among the synthetic shapes and show how the PF-SDM can be interpreted in terms of shape similarities and asymmetries.

3.2 Experiment 2: Robustness

We test the robustness of the PF-SDM to image pre-processing and sampling errors by generating a dataset of 50 augmented images, each containing 10 examples of each of the five test shapes from Fig. 3. The augmented images are

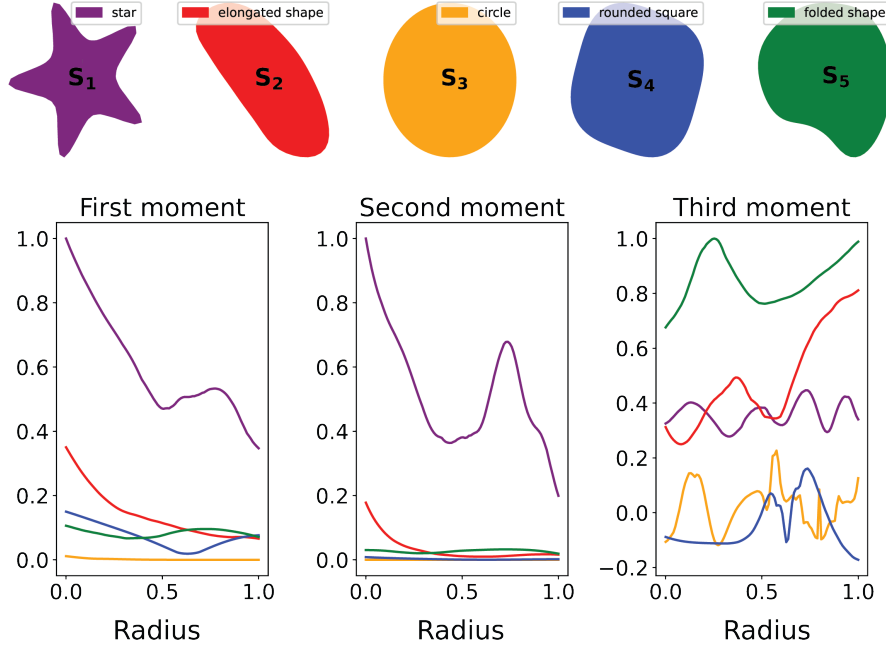


Figure 3: First (left), second (center), and third (right) normalized curvature angular moments as a function of radius for the five test shapes shown on top. Line colors match shape colors.

generated by random translation, rotation, reflection, and scaling. We then visualize the first two principal components of a Principal Component Analysis (PCA) [13] of the vector embeddings of the PF-SDM in Fig. 4 and compare the results with EFA [6] and GPA [12]. We use the following vector space embeddings:

- **PF-SDM:** We compute the third-order distance matrix $D_\phi := (d_\phi^3(S_i, S_j))_{i,j=1}^{50}$, as this order contains the most information about shape asymmetries (see Fig. 3), and use each row as a vector representation for a shape, e.g., $v_{S_\alpha} := (D_{l,\alpha})_{j=1}^{50}$ is the vector representation for the shape S_α , for all $\alpha \in \{1, \dots, 50\}$.
- **EFD:** We compute the coefficients $\mathbf{c} := \{c_{S_1}, \dots, c_{S_{50}}\}$ of the EFD using the `spatial-efd` package [7]. The coefficients are normalized to ensure translation, rotation, and scaling invariance. We construct the distance matrix $D_{\text{EFD}} := (\|c_{S_i} - c_{S_j}\|_2)_{i,j=1}^{50}$ and use each row as a vector representation for a shape.
- **GPA:** We consider a set of 2000 equidistant sampling points $\mathbf{x}^\alpha := (x_{i,\alpha})_{i=1}^{2000} \subseteq S_\alpha$ on each shape S_α . Using the GPA implementation in `SciPy` [20], we align each shape with all others, resulting in the modified points $\tilde{\mathbf{x}}^\alpha := (\tilde{x}_{i,\alpha})_{i=1}^{2000} \subseteq S_\alpha$, and we construct the distance matrix $D_{\text{GPA}} := (\|\tilde{\mathbf{x}}^i - \tilde{\mathbf{x}}^j\|_2)_{i,j=1}^{50}$. Each row of this matrix is used as a vector representation of a shape.
- **GPA + EFD:** We obtain a joint vector representation of GPA+EFD as follows: We use the EFD descriptors with normalized coefficients $\{c_1, \dots, c_{50}\}$ to sample equidistant points $\mathbf{y}^\alpha := (y_{i,\alpha})_{i=1}^N \subseteq S_\alpha$. We apply the GPA to obtain the modified coordinates $\tilde{\mathbf{y}}^\alpha := (\tilde{y}_{i,\alpha})_{i=1}^N \subseteq S_\alpha$ and compute the matrix $D_{\text{Hybrid}} := (\|\tilde{\mathbf{x}}^i - \tilde{\mathbf{x}}^j\|_2)_{i,j=1}^{50}$, the rows of which are the embedding vectors.

For all methods, we use the same image pre-processing, as described in Subsection 2.1. From the results in Fig. 4, we observe that the PF-SDM exhibits the best robustness against shape-preserving affine transformations, as point of the same color (corresponding to transformed version of the same shape) are closer together than in any other tested method. Moreover, the PCA plot for the PF-SDM reveals a hierarchy in the shape clustering. The star shape is the most distant from the others, while the circle and the rounded square are closest together, as intuitively expected. The folded and elongated shapes are more similar to each other than to the rest of the shapes. This shows how the PF-SDM is robust against shape variations yet reveals meaningful clusters.

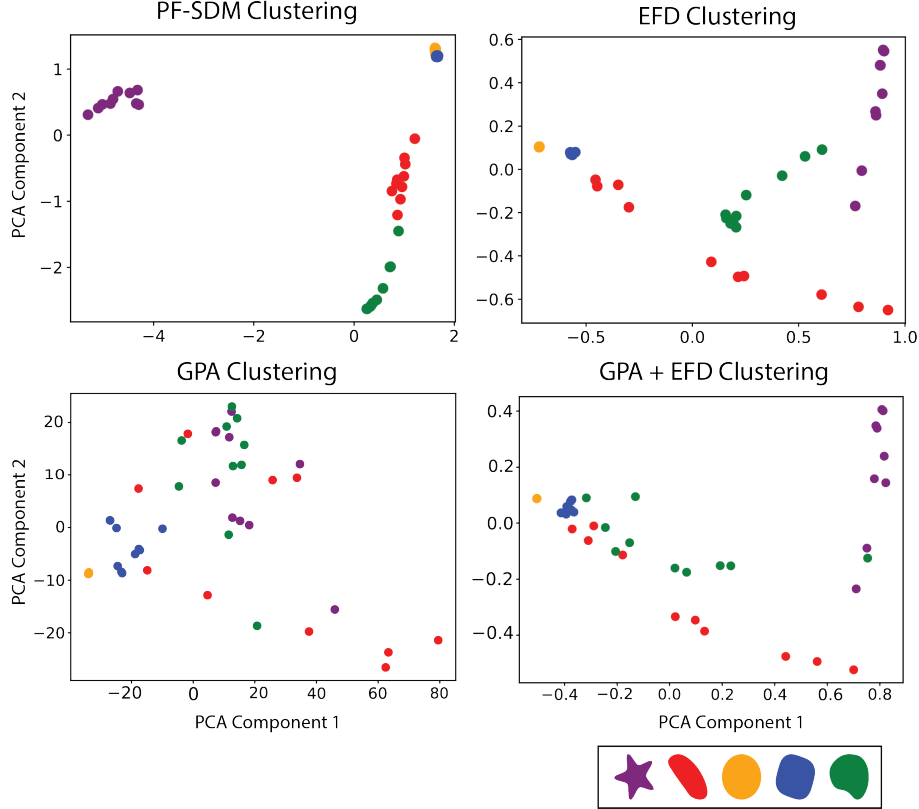


Figure 4: First two principal components of the PF-SDM, EFD, GPA, and combined GPA+EFD morphometrics for the five test shapes shown in the inset legend. Point colors match shape legend colors.

4 Conclusion

We introduced the Push-Forward Signed Distance Morphometric (PF-SDM) as a continuous geometric morphometric, invariant to shape-preserving transformations such as rotation, translation, scaling, and reflection. We provided both the theoretical foundation for PF-SDM and a practical algorithm for its computation. Through experiments on synthetic shapes, we demonstrated that PF-SDM effectively generates hierarchical classifications of geometric objects based on their shapes. Additionally, we showcased its interpretability and robustness compared to established geometric morphometrics like Elliptical Fourier Analysis and Generalized Procrustes Analysis.

For the sake of clarity of notation and simplicity of the exhibition, we considered two-dimensional shapes throughout this manuscript. All concepts do, however, generalize to higher dimensions. More difficult is the generalization from closed shapes to open or not singly connected manifolds, which requires tree or vector SDFs [22, 23]. Future work will extend the PF-SDM to include temporal features, enabling exploration of dynamic shape trajectories. Although we have demonstrated the continuity of the metric, further investigation into its differentiability could open new avenues, such as incorporating the PF-SDM as a loss function in machine learning models to enhance shape analysis. Moreover, the PF-SDM can be generalized to Sobolev norms [18], which could capture further geometrical features of the PF-SDFs. The software and data for this article are available at: <https://git.mpi-cbg.de/mosaic/software/machine-learning/pf-sdm>.

5 Acknowledgments

This work was supported by the German Ministry of Education and Research (BMBF, Bundesministerium für Bildung und Forschung) as part of the Center for Scalable Data Analytics and Artificial Intelligence (ScADS.AI).

References

- [1] Juan-Esteban Suarez Cardona, Phil-Alexander Hofmann, and Michael Hecht. Negative order Sobolev cubatures: preconditioners of partial differential equation learning tasks circumventing numerical stiffness. *Machine Learning: Science and Technology*, 5(3):035029, IOP Publishing, July 2024.
- [2] Lawrence C. Evans. *Partial differential equations*. American Mathematical Society, Providence, RI, 2010.
- [3] Sachin Krishnan Thekke Veetil, Gentian Zavalani, Uwe Hernandez Acosta, Ivo F. Sbalzarini, and Michael Hecht. Global Polynomial Level Sets for Numerical Differential Geometry of Smooth Closed Surfaces. *SIAM Journal on Scientific Computing*, 45(4):A1995–A2018, 2023. <https://epubs.siam.org/doi/full/10.1137/22M1536510>.
- [4] Juan-Esteban Suarez Cardona and Michael Hecht. Polynomial differentiation decreases the training time complexity of physics-informed neural networks and strengthens their approximation power. *Machine Learning: Science and Technology*, 4(4):045005, IOP Publishing, October 2023. <https://dx.doi.org/10.1088/2632-2153/acf97a>.
- [5] Jeffrey M. Manifolds and Differential Geometry. American Mathematical Society, Graduate Studies in Mathematics, Providence, RI, January 2010.
- [6] Frank P. Kuhl and Charles R. Giardina. Elliptic Fourier features of a closed contour. *Computer Graphics and Image Processing*, 18(3):236–258, Elsevier, March 1982. [http://dx.doi.org/10.1016/0146-664X\(82\)90034-X](http://dx.doi.org/10.1016/0146-664X(82)90034-X).
- [7] Stuart W. D. Grieve. spatial-efd: A spatial-aware implementation of elliptical Fourier analysis. *The Journal of Open Source Software*, 2(11):189, The Open Journal, March 2017. <http://dx.doi.org/10.21105/joss.00189>.
- [8] Gary Bradski. The OpenCV Library. *Dr. Dobbs’s Journal of Software Tools*, 2000.
- [9] M. C. Delfour and J. P. Zolesio. Shape Analysis via Oriented Distance Functions. *Journal of Functional Analysis*, 123(1):129–201, Elsevier, July 1994. <http://dx.doi.org/10.1006/jfan.1994.1086>.
- [10] Lennart J. Schulze, Sachin K. T. Veetil, and Ivo F. Sbalzarini. A high-order fully Lagrangian particle level-set method for dynamic surfaces. *Journal of Computational Physics*, 515:113262, 2024. <https://doi.org/10.1016/j.jcp.2024.113262>.
- [11] Andrea Torsello and Edwin R. Hancock. A skeletal measure of 2D shape similarity. *Computer Vision and Image Understanding*, 95(1):1–29, Elsevier, July 2004. <http://dx.doi.org/10.1016/j.cviu.2004.03.006>.
- [12] J. C. Gower. Generalized Procrustes analysis. *Psychometrika*, 40(1):33–51, Springer, March 1975. <http://dx.doi.org/10.1007/BF02291478>.
- [13] Karl Pearson F.R.S. LIII. On lines and planes of closest fit to systems of points in space. *The London, Edinburgh, and Dublin Philosophical Magazine and Journal of Science*, 2(11):559–572, Taylor & Francis, 1901. <http://dx.doi.org/10.1080/14786440109462720>.
- [14] Stanley Osher and Ronald Fedkiw. *Level set methods and dynamic implicit surfaces*. Springer, December 2003.
- [15] J. A. Sethian and A. Vladimirsky. Fast methods for the Eikonal and related Hamilton–Jacobi equations on unstructured meshes. *Proceedings of the National Academy of Sciences*, 97(11):5699–5703, 2000. <http://dx.doi.org/10.1073/pnas.090060097>.
- [16] Alexander Kirillov, Eric Mintun, Nikhila Ravi, Hanzi Mao, Chloe Rolland, Laura Gustafson, Tete Xiao, Spencer Whitehead, Alexander C. Berg, Wan-Yen Lo, Piotr Dollár, and Ross Girshick. Segment Anything. arXiv, 2023. <https://arxiv.org/abs/2304.02643>.
- [17] Stanley Osher and James A. Sethian. Fronts propagating with curvature-dependent speed: Algorithms based on Hamilton–Jacobi formulations. *Journal of Computational Physics*, 79(1):12–49, Elsevier, November 1988. [http://dx.doi.org/10.1016/0021-9991\(88\)90002-2](http://dx.doi.org/10.1016/0021-9991(88)90002-2).
- [18] Raa and Jjff. Preface. In *Sobolev Spaces*, pages ix–xi. Elsevier, 2003.
- [19] Klein et al. Digital Morphometrics of Two North American Grapevines (*Vitis*: Vitaceae) Quantifies Leaf Variation between Species, within Species, and among Individuals. *Frontiers in Plant Science*, 8, Frontiers Media SA, March 2017. <http://dx.doi.org/10.3389/fpls.2017.00373>.
- [20] Virtanen et al. SciPy 1.0: Fundamental Algorithms for Scientific Computing in Python. *Nature Methods*, 17:261–272, 2020. <https://doi.org/10.1038/s41592-019-0686-2>.
- [21] K. Turner, S. Mukherjee, and D. M. Boyer. Persistent homology transform for modeling shapes and surfaces. *Information and Inference*, 3(4):310–344, Oxford University Press, December 2014. <http://dx.doi.org/10.1093/imaiai/iaa011>.

-
- [22] Luminita A. Vese and Tony F. Chan. A Multiphase Level Set Framework for Image Segmentation Using the Mumford and Shah Model. *International Journal of Computer Vision*, 50(3):271–293, Springer, 2002. <http://dx.doi.org/10.1023/A:1020874308076>.
- [23] Xun Xiao, Veikko F. Geyer, Hugo Bowne-Anderson, Jonathon Howard, and Ivo F. Sbalzarini. Automatic optimal filament segmentation with sub-pixel accuracy using generalized linear models and B-spline level-sets. *Medical Image Analysis*, 32:157–172, Elsevier, August 2016. <http://dx.doi.org/10.1016/j.media.2016.03.007>.